Characterization of extracellular vesicles by IR spectroscopy: fast and simple classification based on amide and C-H stretching vibrations

Judith Mihály*, Róbert Deák, Imola Csilla Szigyártó, Attila Bóta, Tamás Beke-Somfai, Zoltán Varga

Institute of Materials and Environmental Chemistry, Research Centre for Natural Sciences of the Hungarian Academy of Sciences, 1117 Budapest, Magyar tudósok körútja 2, Hungary

*Corresponding author.
E-mail address: mihaly.judith@ttk.mta.hu

Abstract

Extracellular vesicles isolated by differential centrifugation from Jurkat T-cell line were investigated by attenuated total reflection Fourier-transform infrared spectroscopy (ATR-FTIR). Amide and C-H stretching band intensity ratios calculated from IR bands, characteristic of protein and lipid components, proved to be distinctive for the different extracellular vesicle subpopulations. This proposed 'spectroscopic protein-to-lipid ratio', combined with the outlined spectrum-analysis protocol is valid also for low sample concentrations (0.15-0.05 mg/ml total protein content) and can carry information about the presence of other non-vesicular formations such as aggregated proteins, lipoproteins and immune complexes. Detailed analysis of IR data reveals compositional changes of extracellular vesicles subpopulations: second derivative spectra suggest changes in protein composition from parent cell towards exosomes favoring proteins with β-turns and unordered motifs at the expense of intermolecular β-sheet structures. The IR-based protein-to-lipid assessment protocol was tested also for red blood cell derived microvesicles for which similar values were obtained. The potential applicability of this technique for fast and efficient characterization of vesicular components is high as the investigated samples require no further preparations and all the different molecular species can be determined in the same sample. The results indicate that ATR-FTIR measurements provide a simple and reproducible method for the screening of extracellular vesicle preparations. It is hoped that this sophisticated technique will have further impact in extracellular vesicle research.

Keywords: *exosome; microvesicle; extracellular vesicles; ATR-FTIR spectroscopy; spectroscopic protein-to-lipid ratio; erythrocyte ghost membrane*

Introduction

Extracellular vesicles (EVs) are lipid bilayer enclosed structures released by cells. EVs generally are classified based on their cellular origin, biogenesis and physicochemical properties [1]. Apoptotic bodies (AB), with a broad size range between 800 – 5000 nm, are generated when cells undergo apoptosis and fragmentation. Microvesicles (MV) are described as being formed by outward budding and fission of the plasma membranes and having particle diameter of 100 – 1000 nm. Exosomes (EXO), with reported diameter between 70 – 150 nm, are produced within the cell and are released through an exocytosis event when multivesicular bodies (MVBs) fuse with the plasma membrane.

EVs have emerged as important mediators of intercellular communication [2-4]. Since EVs have been related to tumorigenesis [5,6], the spread of viruses and pathogenic agents as HIV-1 [7], amyloid-β-derived peptides [8] and α-synuclein [9] (which are pathologically linked to Alzheimer's disease and Parkinson's disease, respectively), they may serve as biomarkers of disease and as potential therapeutic targets. Despite intense investigation, however, many properties and mechanisms remain elusive due to the lack of standardization of isolation and characterization methods which hinders the translation of EV-based diagnostics into clinical use [10].

Considering the above, there is a need for fast, simple and reliable methods for EV characterization. One important issue is the determination of size distribution. Beside current techniques like electron microscopy (cryo-EM or freeze-fracture combined EM) [11,12], flow cytometry [13,14], and dynamic light scattering (DLS) [15], the introduction of novel techniques like nanoparticle tracking analysis (NTA) [16], resistive pulse sensing (RPS), small-angle X-ray scattering (SAXS) or size exclusion chromatography coupled with dynamic light scattering (SEC-DLS) are also ongoing [17,18]. Another key issue in EV research is the total protein determination and characterization by bioanalytical assays [19-21]. Quite recently, the protein-to-lipid ratio measured by combined BCA protein assay and sulfophosphovanillin (SPV) lipid assay as an additional parameter for routine quality control of EV preparation was proposed [22]. Raman spectroscopy, especially Raman tweezers microspectroscopy (RTM) is also a candidate for rapid and label-free characterization of cell-derived extracellular vesicles [23-25].

Infrared (IR) spectroscopy based protein quantification is already commercialized [26] and provide solution for many problems associated with colorimetric assays and UV-Vis detection used in protein research. Moreover, several studies deal with the feasibility of IR spectroscopy-based analytical methods in clinical and diagnostic analysis [27]. Liu et al. [28] proposed a reagent-free method for simultaneous determination of serum cholesterol in HDL and LDL by infrared spectroscopy. More recently, the attenuated total reflection Fourier-transform infrared spectroscopy (ATR-FTIR) was applied to obtain quantitative information about macromolecular composition in adipose tissue as major fat storage depot, and in liver and muscle, which may store ectopic fat [29]. Despite its advantages, ATR-FTIR spectroscopy so far was not used to characterize EV samples. To our best knowledge, our group has been the first who performed exploratory IR study on EVs.

The determination of protein-to-lipid ratio by infrared spectroscopy was first proposed by Navarro et al. [30]. Since proteins and lipids show distinctive absorption bands, the FTIR spectrum can be used to estimate the protein-to-lipid ratio by dividing the relative intensity of amide I protein band around 1650 cm^{-1}, by that of carbonyl stretching of lipid-related ester bonds at around 1725-1740 cm^{-1}. Investigating samples made of diacyl phospholipids and proteins mixed in known ratios they obtained a standard deviation less than ±4% over the lipid-protein molar ratio range of 9:1 to 320:1. ATR-FTIR spectroscopy was also recommended as a rapid method for assessing lipid:protein and detergent:protein ratios in membrane-protein crystallization [31]. Lipid-protein ratios down to approximately five molecules of lipid per molecule of a 300 kDa protein were accurately detected. We have to point out, however, that since the absorption coefficients of the protein- and lipid-related bands are different, for real biological samples without a proper calibration procedure only a 'spectroscopic' protein-to-lipid ratio can be determined [32]. The 'spectroscopic' protein-to-lipid ratio, however, has been successfully applied in realistic measures of differences in protein-to-lipid ratios from one membrane to another investigating thylakoid and cytoplasmic membranes of cyanobacteria [32] or Escherichia coli membranes [33].

The purpose of the present study was to assess the feasibility of ATR-FTIR spectroscopy as a fast and simple method for EV characterization and classification based on peculiar IR bands.

1. Materials and methods

1.1. Materials

Phospholipids and Brain Total Lipid Extract were purchased from NOF Corp., and Avanti Polar Lipids Inc., respectively. Cholesterol (Chol) and bovine serum albumin (BSA) used as protein standard were purchased from Sigma Aldrich. BSA – lipid mixtures in PBS buffer with varying protein-to-lipid ratios (from 0.2 to 4 mg/ml) were prepared from Brain Total Lipid Extract and a lipid mixture of Cholesterol, 1,2-dipalmitoyl-*sn*-glycero-3-phosphocholine (DPPC), 1,2-dioleoyl-*sn*-glycero-3-phosphocholine (DOPC), 1,2-dipalmitoyl-*sn*-glycero-3-phosphoethanolamine (DPPE), 1,2-dipalmitoyl-sn-glycero-3-phosphoserine, sodium salt (DPPS) with Chol:DPPC:DOPC:DPPE:DPPS=5:1:1:2:1 composition, respectively by thin-film hydration method.

1.2. Preparation of model vesicles and EV samples

1.2.1. DOPC-BSA liposome preparation:
To investigate the possible effect of protein or lipid adsorption on the ATR crystal on IR spectroscopy based protein-to-lipid ratio, bovine serum albumin (BSA) loaded 1,2-dioleoyl-*sn*-glycero-3-phosphocholine (DOPC) liposomes as simple models of EVs were investigated. DOPC and BSA was mixed in 1:1 weight ratio and solved in PBS buffer solution (1.3 mg/ml final concentration). To achieve homogenous mixture and the maximal loading capacity, repeated heating (37°C) and cooling (-196°C) steps were applied. 1-1 ml from the stock solution was extruded through 600, 200 and 80 nm pore sized membrane, respectively. The unilamellar vesicles were purified from the soluble proteins by Sepharose CL-4B (GE Healthcare) gelfiltration.

1.2.2. Ghost membrane preparation:
Erythrocyte ghosts were prepared from freshly outdated erythrocyte concentrate (from Hungarian National Blood Transfusion Service). For a single isolation 4 ml of the pure cell suspension was tenfold diluted with lysis buffer (5 mM, pH: 8, TRIS buffer). The empty membranes were washed 4-5 times with an Avanti J26XP centrifuge, 10000 rpm to achieve haemoglobin free ghosts. The final ghost pellet was suspended in isotonic PBS buffer.

1.2.3. EV isolation:
Apoptotic bodies, microvesicles and exosomes were isolated from Jurkat T-cell line cell culture. RPMI-1640 medium containing 10% fetal bovine serum (FBS), 1% glutamine and 1% penicillin/streptomycin was used as growing medium. The collection of vesicles started when approximately 10^7 cell numbers was reached. At that time the cell medium was replaced with an FBS free one, in order to avoid the sample contamination with bovine serum microvesicles. Jurkat cells were incubated in FBS free "collecting medium" for 24 hours. Collecting medium contained 1μM doxorubicin, for apoptosis induction.
EV isolation was performed by following the commonly used ultracentrifugation protocol guidelines. As a first step the removal of the cells and cell debris was achieved by two

consecutive sedimentations (Nüve NF800R centrifuge, 300g, 5 min). The supernatant was submitted to a 3000g centrifugation for 30 min to pellet apoptotic bodies. The supernatant was next ultracentrifuged at 20000g for 30 min to pellet microvesicles (Thermo Sorwall WX ultra centrifuge, with Thermo Sorwall 1270 fixed angle titanium rotor). Finally, exosomes sedimentation was performed by ultracentrifugation by 110000g for 1h. All pellets were washed with isotonic PBS buffer and the final pellets were suspended in 200 μl PBS. 4 independent isolations (JK1-JK4) were performed.
Erythrocyte derived EVs were isolated from the same freshly outdated erythrocyte concentrate as used for ghost membrane preparation (from Hungarian National Blood Transfusion Service). According to the literature erythrocytes produce large amount of microvesicles during their lifetime, as they use shedding microvesicles to get rid of the excess membrane components [34]. The cell suspension was diluted to double volume with isotonic PBS buffer, the cells were sedimented and used for erythrocyte ghost preparation, while their supernatant was used for microvesicle isolation. After two consecutive sedimentations (Nüve NF800R centrifuge, 1500rpm, 10 min) the supernatant was submitted to a 20000g (Thermo Sorwall WX ultra centrifuge, with Thermo Sorwall 1270 fixed angle titanium rotor) centrifugation for 30 min. The pellets were washed with isotonic PBS buffer, than the final pellet was suspended in 200 μl PBS.

1.3. Freeze-fracture transmission electron microscopy (FF-TEM)

FF-TEM allows the study of the morphology of EVs in their native environment, by rapid freezing of the sample and without any fixation or negative staining materials [18]. The vesicles samples were mixed with glycerol (sample:glycerol at 3:1 volume ratio) to avoid freezing artifacts. Approximately 1 μl of sample was pipetted onto a golden sample holder and suddenly frozen in liquid freon at -194°C, then stored in liquid nitrogen. Fracturing was performed at -100°C in a Balzers freeze-fracture device (Balzers BAF 400D, Balzers AG, Liechtenstein). Replicas from the fractured surfaces were made by carbon-platinum shadowing, then washed with surfactant solution and distilled water. The replicas were placed on 200 mesh copper grid and examined in a MORGAGNI 268D (FEI, The Netherlands) transmission electron microscope.

1.4. Dynamic light scattering (DLS)

The measurement of the average size and size distribution of the isolated EV and reference samples was carried out by an AvidNano W130i dynamic light scattering apparatus (AvidNano, UK). 80 μl samples were used in a low-volume cuvette (UVette, Eppendorf Austria GmbH). The analysis of the measurement data was performed using the i-Size 3.0 software.

1.5. Protein concentration determination by Bradford assay

Total protein content of samples was determined using the Bio-Rad Protein Assay, based on Bradford's method that involves the binding of Coomassie Brilliant Blue G-250 dye to proteins. Bovine Serum Albumin (BioRad Laboratories, USA) was used as standard (2 mg/ml). To 0.5 ml of each standard (0-25 μg/ml) and unknown sample solution were added

0.5 ml dye reagent and was vortex for 15 sec. The samples were incubated at room temperature for at least 5 min and the absorbance was measured at 595 nm.

All UV-Vis measurements were done at 25ºC using a Hewlett-Packard 8453 diode array UV-Vis spectrophotometer thermostated with Grant LTD 6G circulating water bath, in a quartz cuvette with a 1 cm optical path.

1.6. Attenuated total reflection Fourier-transform infrared spectroscopy (ATR-FTIR)

ATR-FTIR spectra were collected using a Varian 2000 FTIR Scimitar Series spectrometer (Varian Inc, USA) equipped with a liquid nitrogen cooled mercury-cadmium-telluride (MCT) detector and with a 'Golden Gate' single reflection diamond ATR accessory (Specac Ltd, UK). 5 μl of sample was mounted on the diamond ATR crystal and a thin dry film was obtained by slowly evaporation of the buffer solvent under ambient conditions [33]. The measurements were performed at room temperature, immediately after drying the sample (within approximately 5 minutes). 128 scans were co-added at a nominal resolution of 4 cm^{-1}. After each data acquisition ATR correction was performed. For all spectral manipulation the GRAMS/32 software package (Galactic Inc, USA) was used.

1.7. Statistical analysis

For data analysis we used the GraphPad Prism 5.0 software. For comparison of protein-to-lipid parameter of different EV subpopulations unpaired t-tests were run, followed by one-way ANOVA. P values less than 0.05 were considered statistically significant.

2. Results and discussion

2.3. Characterization of EVs

Figure 1A shows typical TEM pictures of freeze-fracture replicas of the isolated EV subpopulations derived from Jurkat cells. Spherical vesicles with granular fractured surfaces, presumably proteins or protein aggregates, are observed for all EV subpopulations. The average diameters fall around 100 nm, 200 nm and 1μm for exosomes, microvesicles and apoptotic bodies, respectively. These values coincide with the size distribution measured by DLS (**Figure 1B**) and are in agreement with the typical values reported in literature [2].

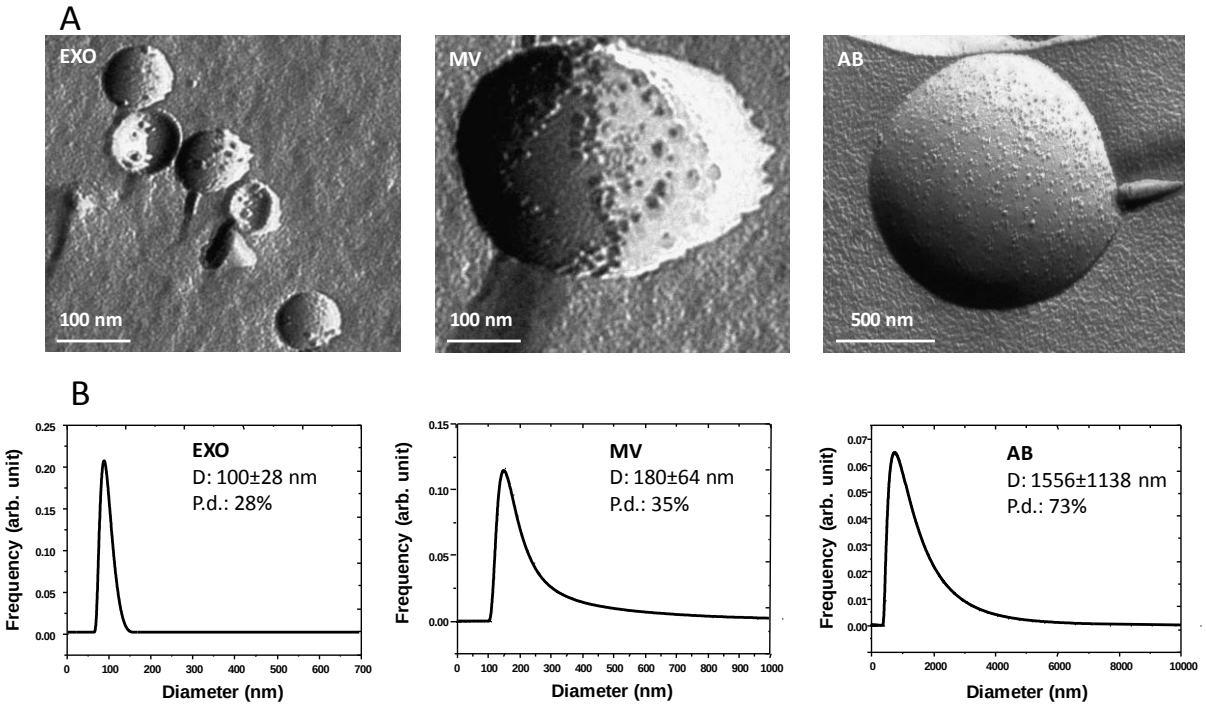

Fig.1 (A) Typical FF-TEM pictures of Jurkat cell derived EV subpopulations. (B) Size distribution measured by dynamic light scattering (DLS) measured for the same EV subpopulations. D: mean diameter; P.d.: polydispersity.

Beside the classification of EVs based on morphological criteria, accurate control of EV concentration is requirement to characterize EV isolation. One of the most used techniques is to quantify the EVs by quantification of total proteins [35] by protein assays. Total protein contents of the different EV subpopulation determined using Bradford assay with the Bio-Rad Protein Assay Reagent are presented in Table 1.

Table 1. Total protein content (with standard deviations) of Jurkat cell derived EV subpopulations (n=4 independent isolation).

EV	**EXO** (±SD)	**MV** (±SD)	**AB** (±SD)
Total protein content (mg/ml)	0.051±0.02	0.053±0.03	0.124±0.02

2.4. IR spectra of different EV subpopulations

Representative IR spectra of different EV subpopulations derived from Jurkat-cell line, together with the spectrum of original cell line are presented in **Figure 2A**.

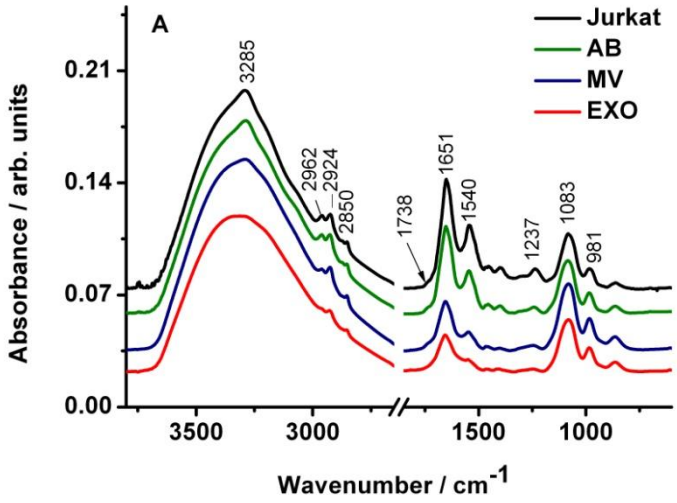
A
Jurkat
AB
MV
EXO
3285
2962
2924
2850
1738
1651
1540
1237
1083
981
0.21
0.14
0.07
0.00
3500
3000
1500
1000
Absorbance / arb. units
Wavenumber / cm-1

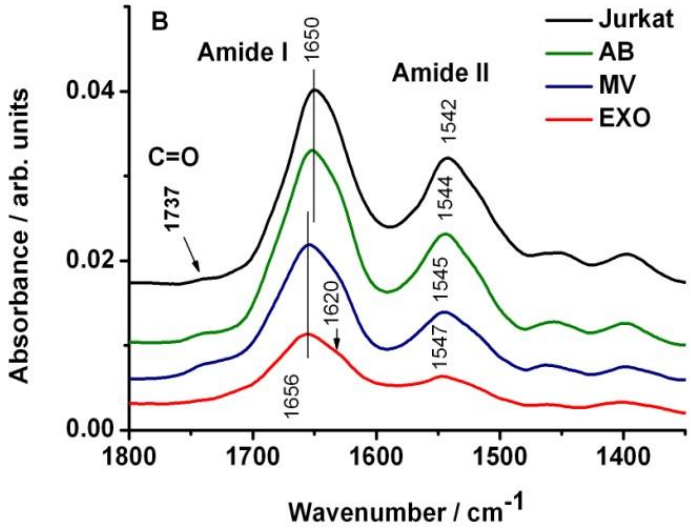
B
Jurkat
AB
MV
EXO
Amide I
1650
Amide II
1542
C=O
1737
1544
1545
1620
1547
1656
0.04
0.02
0.00
1800
1700
1600
1500
1400
Absorbance / arb. units
Wavenumber / cm-1

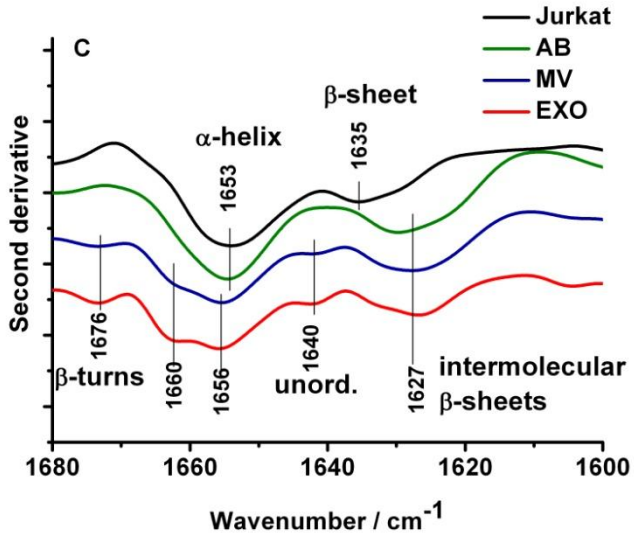
C
Jurkat
AB
MV
EXO
β-sheet
α-helix
1635
1653
1676
1660
1656
1640
1627
β-turns
unord.
intermolecular
β-sheets
1680
1660
1640
1620
1600
Second derivative
Wavenumber / cm-1

Fig.2 (A) Representative ATR-FTIR spectra of EVs isolated by differential centrifugation from Jurkat cell line. (B) Representative ATR-FTIR spectra of EVs after PBS buffer subtraction in the 1800-1350 cm^{-1} wavenumber region: C=O stretching from lipid esters, amide I and amide II bands of proteins. (C) Second derivative IR spectra of the amide I region for protein secondary structure assessing.

From the IR spectra one can gather general information concerning the molecular constituents and their structures (**Figure 2A**). The main features of the spectra, common for all biological samples, are the two prominent amide absorptions, around 1651 cm^{-1} (termed amide I, originating mainly from C=O stretching vibrations of the protein peptide backbone) and another at 1540 cm^{-1} (termed amide II, arising from N-H bending vibrations of the peptide groups). The strong band at 3285 cm^{-1} (better observable in the spectra of the original cell line and of the apoptotic body, too) superposed with the broad, overlapped -OH stretching vibrations, belongs to the N-H stretching vibrations of the peptide groups of proteins (termed amide A). The distinct lipid absorption appears around 1738 cm^{-1} originates from the ester groups of phospholipids, triglycerids and cholesterol esters, together with the dominant antisymmetric and symmetric stretching vibrations of the lipid acyl CH_2 groups corresponding to the bands at 2924 and 2850 cm^{-1}, respectively. The absorption band at 1453 cm^{-1} belongs to the bending (scissoring) vibration of lipid acyl CH_2 groups, while the band at 1394 cm^{-1} is attributed to bending vibrations of both lipid and protein CH_3 groups. Bands from the spectral region of 1200-950 cm^{-1} generally are attributed to the stretching vibrations of the phosphodiester groups of phospholipids and to the C-O-C stretching vibrations of phospholipids, triglycerides and cholesterol esters. In our case, however, this spectral region is completely masked by the broad phosphate vibrations bands of the isotonic PBS buffer. Due to the used separation procedure of the different EV subpopulations, i.e. consecutive centrifugation, sedimentation and washing with PBS, a decrease in EV concentration of the investigated samples occurs (see **Table 1**). The very low sample concentration (around 0.05 mg/ml total protein) results in a comparable intensities of IR absorption bands of buffer (PBS) molecules with that of EVs. Consequently, the subtraction of pure PBS dry film spectra is required prior to further analysis of EV samples.

Detailed analysis of spectral region from 1800 to 1350 cm^{-1} for different EV subpopulations (**Figure 2B**) reveals subtle changes in the shape and relative intensity of amide I and lipid-related ester C=O stretching vibrations. The amide I region (1700-1600 cm^{-1}) is used for the secondary structure determination of the proteins. The broad envelope of the amide I can be resolved to individual band components, which can be used to characterize the α-helical, β-sheet, random, etc. content of the given proteins [36]. Protein secondary structure for EV subpopulations were assessed by second derivative IR spectra of amide I band (**Figure 2C**). As to the EVs, going towards exosomes changes in protein composition can be witnessed favoring β-turns (band component at 1676 cm^{-1}) and unordered protein motifs (1640 cm^{-1}) at the expense of β-sheet conformations (1635 cm^{-1}) [37,38]. As to the MV and EXO spectra, the arising band component around 1627 cm^{-1}, characteristic of non-native intermolecular β-sheets, suggests the presence of aggregated proteins or apolipoproteins [37,39]. The new band

component at 1660 cm^{-1} might be related to triple-helix structure characteristic for some immune complexes [40] or associated with nucleic acid (RNA) content of the EVs [41].

It is worth to note that the spectral features of parent Jurkat cells and apoptotic bodies are very similar suggesting their similar composition. For microvesicles (MV) the relative intensity of the carbonyl stretching bands is higher indicating its higher content of phospholipids presumably due to their plasma membrane origin. In the case of exosomes, however, the C=O stretching band intensity is suppressed. This is in accordance with the observation that exosomes from a variety of cells are highly enriched in cholesterol, sphingomyelin, and ceramide at the expense of phosphatidylcholine and phosphatidylethanolamine [3].

2.5. Protein-to-lipid ratio

Due to the impact of IR spectroscopy to study simultaneously protein and lipid components a 'spectroscopic protein-to-lipid ratio' can be derived by dividing the relative intensities of amide I protein band by that of carbonyl stretching bands of lipid-related ester bonds [32]. As an initial step we derived P/L ratios based on relative intensities of amide I and carbonyl stretchings (**Figure S1**, Supplement). The results are in close agreement regarding the changes of P/L values among subpopulation of extracellular vesicles with a recently applied method based on a combination of sulfophosphovanillin (SPV) total lipid assay and micro BCA protein assay [22, 42].

Note, however, that in order to exploit full potential of the ATR-FTIR techniques, including high reproducibility, relative comparison of intensities of amide I and lipid-related carbonyl stretching bands encounters several difficulties. The very low concentration of as-prepared EV samples (usually between 0.15-0.05 mg/ml, determined by Bradford assay) demands very sensitive FTIR technique. Our single reflection diamond ATR accessory, however, suits the requirement. Another important issue is the possible presence of non-vesicular materials like aggregated proteins, amino acids, etc. To overcome this problem, the integrated amide I band intensity will be determined by curve fitting with the Lorentz-function of the 1653 cm^{-1} band component. In this way false values due to additional band components of amino acids (around 1599 cm^{-1}) and of aggregated proteins or apolipoproteins (band component at 1622 cm^{-1}) [28,39] can be omitted. Concerning the lipid content determination from the EVs' spectra, the carbonyl stretching of lipid esters are of very low intensity, hence inaccurate for reliable protein-to-lipid characterization. Moreover, our preliminary spectroscopic P/L values using the lipid-related carbonyl stretching band were not significantly distinguishing for EXO and MV subpopulations (**Table S1**, Supplement).

Therefore, here an alternative vibration, characteristic for lipid species, the integrated intensity of CH_2/CH_3 stretching vibrations (3040-2700 cm^{-1}) was chosen for in depth evaluation. The spectrum in the 3500-2700 cm^{-1} wavenumber region is dominated by the strong broad band of water –OH stretching vibration. After PBS buffer background subtraction, however, the asymmetric and symmetric stretching vibrations of CH_2 and CH_3 groups, corresponding mainly to lipid chains, emerge. The olefinic =CH stretching bands arising from unsaturated lipid chains (around 3010 cm^{-1}) is also included in the integration zone. Moreover, using the C-H stretching region the impact of sterols, like cholesterol, often

enriched in exosome membranes [3,25], can be taken also into account. Proteins have also a very minor contribution to the integrated intensity of the C-H stretching region, however, as we use a ratio of integrated intensities this contribution of proteinic C-H stretching is compensated (showed also by the linear fit in standard plots in **Figure S2** and **S3**).

The spectral evaluation protocol consists of the following successive steps:

1. Subtraction of PBS buffer dry film spectra.
2. Baseline correction.
3. Smoothing procedure (Savitsky-Golay method (third grade polynomial, 5 smoothing points).
4. Determination of protein content by fitting of the amide I band with Lorentzian component bands. For EV samples sufficient fit was achieved by using two components: one centered around 1653 cm^{-1}, the other around 1600-1620 cm^{-1}. The latest might belong to aggregated proteins, amino acid residues, etc. For protein-to-lipid calculation the integrated area of the band component centered at 1656 cm^{-1} was invoked (**A(Amide I)**).
5. Determination of lipid content by total integrated intensity of CH_2/CH_3 stretching vibration from 3040 to 2700 cm^{-1} (**A(CH_2/CH_3)**).
6. Calculation of 'spectroscopic protein-to-lipid ratio': **P/L_{spectr} = A(Amide I) / A(CH_2/CH_3)**.

To illustrate the process of P/L_{spectr}, the 3040-2700 cm^{-1} (**Figure 3A**) and the 1750-1500 cm^{-1} (**Figure 3B**) regions for a 'contaminated' Jurkat cell derived EV sample are shown.

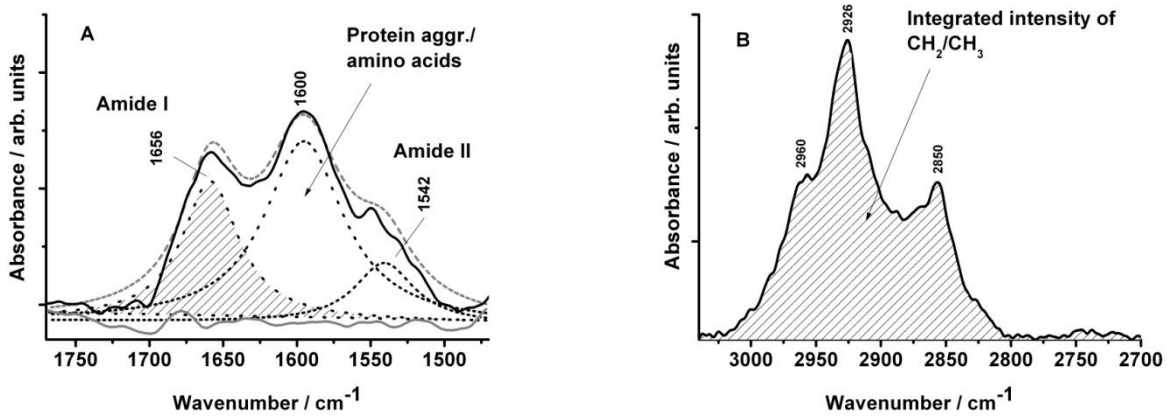

Fig.3 Selected wavenumber regions of a 'contaminated' Jurkat cell derived exosome (isolation JK4) used for P/L determination protocol: (A) amide I and amide II wavenumber region (1770-1470 cm^{-1}) deconvoluted by curve fitting with Lorentz-function (band denoted by dotted lines), (B) C-H stretching region (3040-2700 cm^{-1}) acting for lipid components.

Calculated spectroscopic protein-to-lipid values for Jurkat cell lines derived EVs are presented in **Table 2**, while mean values are shown in **Figure 4.**

Table 2. Spectroscopic protein-to-lipid values calculated for Jurkat cell line derived EVs. JK(1-4) refer to the 4 independent EV isolations. A(Amide I) and A(CH_2/CH_3) denote the

integrated area of selected amide I band and that of C-H stretching region characteristic for protein and lipid components, respectively.

EV	**Spectroscopic P/L** **A(Amide I) / A(CH_2/CH_3)**				
	JK1	**JK2**	**JK3**	**JK4**	**JK mean** (SD, n=4)
EXO	0.73	0.83	0.78	0.84	**0.79**±0.05
MV	0.57	0.65	0.61	0.56	**0.60**±0.04
AB	1.08	1.36	1.19	1.18	**1.20**±0.12

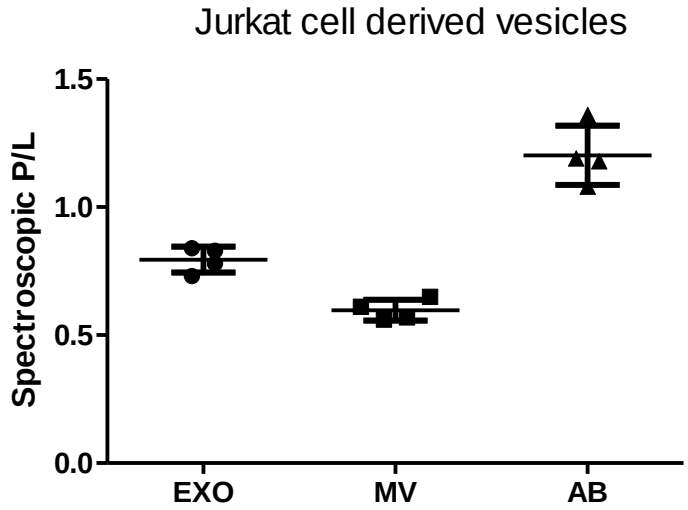

Fig.4 Relative intensities of amide I to C-H stretching bands providing the spectroscopic P/L for Jurkat cell line derived EVs. Mean values are presented by horizontal lines, error bars mark denotes the standard error of the mean (SEM).

Comparing 'spectroscopic P/L' values (**Figure 4**) significant differences were found between the subpopulations of Jurkat cell derived EVs (one-way ANOVA, ****P<0.0001). The highest spectroscopic P/L appears for the apoptotic body. Performing the spectral evaluation protocol for parent cells, usually the P/L_{spectr} values are above 1. It is interesting to note that P/L_{spectr} values for AB subpopulation present the highest standard errors of the means, connected probably to their origin (cell clearance). The real extracellular vesicles, exosomes and microvesicles, both lipid bilayer enclosed structures, show a higher relative amount of lipid component. Interestingly, based on the P/L_{spectr} values the content of lipid is higher for MV samples compared to the EXO ones.

Reliability of the method

2.5.1. Normal probability plots

BSA – lipid mixtures of protein-to-lipid ratios varying from 0.2 to 4 mg/ml were prepared. As the lipid component, we used both a mixture of cholesterol and different phospholipids with the composition of Chol:DPPC:DOPC:DPPE:DPPS=5:1:1:2:1 (relative weights) and Brain

Total Lipid Extract, respectively. The integrated intensity ratio of selected amide I band and of C-H stretching region (A(Amide I) / A(CH_2/CH_3) was determined using the above protocol for each sample and plotted against the known protein-to-lipid ratios. In both cases the plots obtained were best fit by straight line with linear regression correlation coefficients of 0.98675 (for lipid mixture) and 0.99084 (for Brain Total Lipid Extract), respectively (**Figures S2 and S3**, Supplement).

2.5.2. Possible interference of vesicle size and ATR-FTIR technique

Prior to draw structure / composition related conclusion from the distinct protein-to-lipid values for the different subpopulations of EVs, we inspected the eventual biases due to the ATR technique. One bias is related to the potential adsorption of proteins onto the ATR crystal, which may falsify the quantitative estimation of protein concentration from the peak height of the amide I band [43]. In order to test the effect of colloidal aspects / protein encapsulation on the proposed ATR-FTIR based protocol, we investigated BSA loaded DOPC model liposomes with 600, 200 and 80 nm size, corresponding roughly to different EV subpopulations of apoptotic bodies, microvesicles and exosomes, respectively. We calculated the spectroscopic protein-to-lipid values for extruded and gelfiltrated DOPC-BSA vesicles using ATR-FTIR spectra: with increasing vesicle diameter the spectroscopic P/L value also slightly increases. We have to point, however, that all variations are within the error of the measurement and evaluation protocol with no significant differences between the mean P/L values (**Figure S4 and Table S4,** Supplement). Deviations in P/L values promoted by sonication treatment of the sample were also negligible (**Figure S4 and Table S4,** Supplement). So, regarding the trend in spectroscopic P/L values for different EV subpopulation we can rule out the possible interference of vesicle size and/or encapsulated proteins with the ATR-FTIR technique.

2.6. Application to erythrocyte derived EVs

Erythrocyte derived EVs (MVs) were isolated from red blood cell concentrates. For comparison, red blood cell ghost membranes were also prepared (**Figure S5**, Supplement). Calculated ATR-FTIR based protein-to-lipid ratios are presented in **Table 3**.

Table 3. Spectroscopic protein-to-lipid values calculated for red blood cell (RBC) derived MVs (3 independent isolations: RBC1-RBC3), compared with that of ghost membrane prepared from the same RBS concentrate. A(Amide I) and A(CH2/CH3) denote the integrated area of selected amide I band and that of C-H stretching region characteristic for protein and lipid components, respectively.

EV	**Spectroscopic P/L** $\mathbf{A(Amide\ I) / A(CH_2/CH_3)}$			
	RBC1	**RBC2**	**RBC3**	**RBC mean** (SD, n=3)
MV	0.54	0.75	0.53	**0.61**±0.13
Ghost membrane	0.91	0.88	0.91	**0.90**±0.02

Spectroscopic P/L values for erythrocyte derived MVs resemble the mean P/L_{spectr} values determined for MVs originated from Jurkat cells. Unpaired t-test statistical analysis provided also that no statistically difference exist ($P<0.05$) between the mean spectroscopic P/L values of the MV samples of different origin (**Figure S6**). For curiosity, P/L_{spectr} for ghost membranes prepared from the same freshly outdated erythrocyte concentrate was also calculated. The P/L values for RBC ghost membrane are higher than for RBC derived MVs, likely due to the high level of integral and peripheral proteins [44]. Detailed analysis of IR spectra reveals not only differences in the P/L ratio, but also in the protein content of erythrocyte derived MVs and ghosts as shown by the spectral feature of the amide I protein band (**Figure 5A and B**).

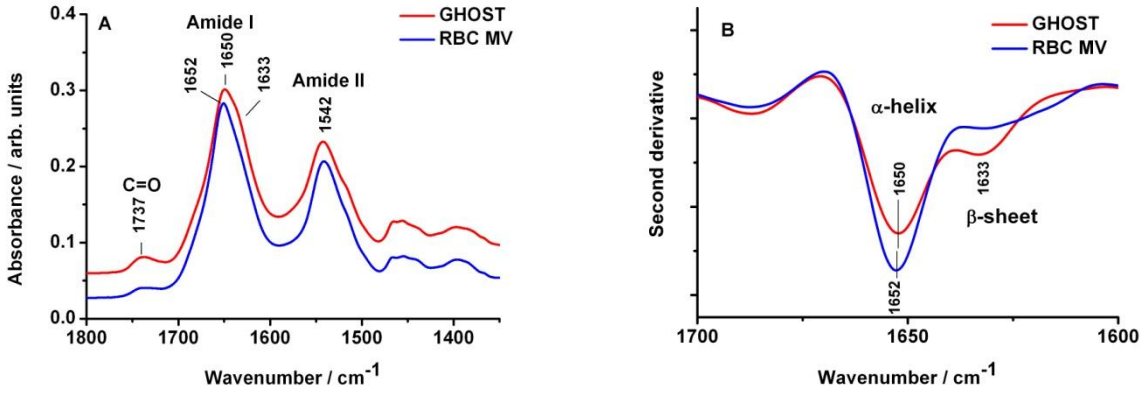

Fig.5 (A) Representative ATR-FTIR spectrum of RBC derived MV (blue line) compared with RBC ghost membrane spectrum (red line). (B) Second derivative IR spectra of the amide I region for protein secondary structure assessing.

Figure 5B shows the second derivatives of the amide I region: regarding the secondary structure of the proteins the α-helix structure is dominant for RBC derived MV sample. The slight shift of the main amide I band component peak suggests that the original membrane milieu of proteins in MV are also changed. Our previous experiences on ghost membrane vesicularisation by physicochemical treatments (sonication and extrusion) resulted in similar

observations with decreased protein-to-lipid ratio [45]. This observation corroborates that EVs are designed naturally vesicles with controlled protein and lipid content resulting in established protein-to-lipid ratios. Moreover, it is interesting to note that artificial nanoerythrosomes, obtained by sonication and extrusion of RBC ghost membrane, with 200 nm average diameter, provide P/L_{spectr} values (P/L_{spectr}=0.59±0.13) [45] close to P/L_{spectr} of natural RBC microvesicles (P/L=0.61±0.13). This implies the adaptability of artificially designed nanoerythrosomes as reference materials for EV characterization and standardization.

Conclusion

In this study we demonstrate the utility of ATR-FTIR spectroscopy to investigate different subpopulations of EVs. The typical IR spectra of apoptotic bodies resemble to those of the parent cells. For exosomes and microvesicles, however, subtle changes in the spectral features of amide I band connected to protein secondary structure was noticed. As to the Jurkat cell derived EXO and MV, band components related to nonnative intermolecular β-sheets, β-turns and unordered protein motifs can be witnessed. These protein structures imply the presence of aggregated proteins, apolipoproteins, triple-helix structures related probably to 'contaminants' like immune complexes, lipoproteins, etc. Interestingly, for red blood cell derived EV samples the α-helix protein structure was dominant.

Furthermore, we introduced the spectroscopic P/L value based on relative intensity of amide I and C-H stretching bands, which is characteristic for different EV subpopulations and thus leading to a simple and fast classification of the studied liposome species. By careful spectral analysis and by employing an advanced IR-based protocol the low concentration range of EVs and the presence of non-desired contaminants, e.g. protein complexes, aggregates, lipoproteins can be overcome. The use of the ATR-FTIR technique provides fast and good quality IR spectra, while requires only minimal amount of sample, usually 3-5 μl, and no sample preparation. Beside the simplicity of the estimation of protein-to-lipid ratio by ATR FTIR spectroscopy, a further advantage of the technique is that both quantities (protein and lipid quantity-related IR band intensities) are obtained from the same experiment. In such a way the experimental error is significantly reduced. However, we have to emphasise that the IR-based protein-to-lipid ratio is not an absolute value but reflects the differences in protein-to-lipid ratios from one biological species to another (i.e. EV subpopulations).

Our results suggest that IR spectroscopy might have a useful role in EV research offering efficient classification of extracellular vesicle subpopulations. The ATR-FTIR method potentially represents a reliable, fast and relatively cheap screening approach for EV isolation.

Acknowledgements

We greatly acknowledge Prof. Edit I. Buzás and Xabier Osteikoetxea for their precious advices and discussions. We thank Teréz Kiss for the FF-TEM pictures. The work was supported by the János Bolyai Research Scholarship of the Hungarian Academy of Sciences.

[1] R. van der Meel, M.H.A.M. Fens, P. Vader, W.W. van Solinger, O. Eniola-Adefeso, R.M. Schiffelers, Extracellular vesicles as drug delivery systems: Lessons from the liposome field, J. Control. Release 195 (2014) 72-85.

[2] B. György, T.G. Szabó, M. Pásztói, Zs. Pál, P. Misják, B. Aradi, V. László, É. Pállinger, E. Pap, Á. Kittel, Gy. Nagy, A. Falus, E.I. Buzás, Membrane vesicles, current state-of-the-art: emerging role of extracellular vesicles, Cell. Mol. Life Sci. 68 (2011) 2667–2688.

[3] G. Raposo, W. Stoorvogel, Extracellular vesicles: Exosomes, microvesicles, and friends, J. Cell Biol. (2013) 200:373-383.

[4] A.M. Janas, K. Sapoń, T. Janas, M.H.B. Stowell, T. Janas, Exosomes and other extracellular vesicles in neural cells and neurodegenerative diseases, BBA-Biomembranes 1858 (2016) 1139.

[5] M. Verma, T.K. Lam, E. Hebert, R.L. Divi, Extracellular vesicles: potential applications in cancer diagnosis, prognosis, and epidemology, BMC Clinical Pathology 15 (2015) 6. doi:10.1186/s12907-015-0005-5

[6] S.A. Melo, L.B. Muecke, Ch. Kahlert, A.F. Fernandez, S.T. Gammon, J. Kaye, V.S. LeBleu, E.A. Mittendorf, J. Weitz, N. Rahbari, Ch. Reissfelder, Ch. Pilarsky, M.F. Fraga, D. Piwnica-Worms, R. Kalluri, Glypican-1 identifies cancer exosomes and detect early pancreatic cancer, Nature 523 (2015) 177.

[7] M. Mack, Transfer of the chemikinine receptor CCR5 between cells by membrane-derived microparticles: a mechanism for cellular human immonodeficiency virus 1 infection. Nature Med. 6 (2000) 769-775.

[8] S.A. Bellingham, B.B. Guo, B.M. Coleman, A.F. Hill, Exosomes: vehicles for the transfer of toxic proteins associated with neurodegenerative diseases? Frontiers Physiol. 3 (2012) 124. http://dx.doi.org/10.3389/fphys.2012.00124

[9] E. Emmanouilidou, Cell-produced α-nuclein is secreted in a calcium-dependent manner by exosomes and impacts neuronal survival. J. Neurosci. 2010; 30: 6838-6851.

[10] S.E.L. Andaloussi, I. Mager, X.O. Breakefield, M.J.A. Wood, Extracellular vesicles: biology and emerging therapeutic opportuinities, Nature reviews, 12 (2013) 347-357.

[11] F. Lavialle, S. Gonnet, E. Larquet, S.G. Kruglik, N. Boisset, R. Daniel, A. Alfsen, I. Tatischeff, Nanovesicles released by Dicytistelium cells: a potential carrier for drug delivery, Int. J. Pahrm. 380 (2009) 206-215.

[12] A. Poliakov, M. Spilman, T. Dokland, C.L. Amling, J.A. Mobley, Structural heterogeneity and protein composition of exosome-like vesicles (prostasomes) in human semen, Prostate, 69 (2009) 159-167.

[13] E.J. van der Vlist, E.N. Nolte-'t Hoen, W. Stoorvogel, G.J. Arkesteijn, M.H. Wauben, Fluorescent labeling of nano-sized sevicles released by cells and subsequent quantitative and qualitative analysis by high-resolution flow cytometry, Nat. Protoc. 7 (2012) 1311-1326, http://dx.doi.org/10.1038/nprot.2012.065

[14] V. Pospichalova, J. Svoboda, Z. Dave, A. Kotrbova, K. Kaiser, D. Klemova, L. Ilkovics, A. Hampl, I. Crha, E. Jandakova, L. Minar, V. Weinberger, V. Bryja, Simplified protocol for flow cytometry analysis of fluorescently labeled exosomes and microvesicles using dedicated flow cytometer, Journal of Extracellular Vesicles 2015, 4: 25530 - http://dx.doi.org/10.3402/jev.v4.25530

[15] V. Palmieri, D. Lucchetti, I. Gatto, A. Maiorana, M. Marcantoni, G. Maulucci, M. Papi, R. Pola, M. De Spirito, A. Sgambato, Dynamic light scattering for the characterization and counting of extracellular vesicles: a powerful noninvasive tool, J. Nanopart. Res. 16 (2014) 2583, doi 10.1007/s11051-014-2583-z

[16] C. Gardiner, Y.J. Ferreira, R.A. Dragovics, C.W. Redman, I.L. Sargent, Extracellular cesicle sizing and enumeration by nanoparticle trackink analysis, J. Extracell. Vesicles, 2 (2013) 19671, doi: http://dx.doi.org/10.3402/jev.v2i0.19671.

[17] E. van der Pol, F. Coumans, Z. Varga, M. Krumrey, R. Nieuwland, Innovation in detection of microparticles and exosomes, J. Thromb. Haemost. 11 (Suppl.1) (2013) 36-45. DOI: 10.111/jth.12254

[18] Z. Varga, Y. Yuana, A.E. Grootemaat, E. van der Pol, C. Gollwitzer, M. Krumrey, R. Nieuwland, Towards traceable size determination of extracellular vesicles, J. Extracell. Vesicles 3 (2014) 23298 http://dx.doi.org/10.3402/jev.v3.23298.

[19] E. van der Pol, A.W. Coumans, A.E. Grootemaat, C. Gardiner, I.L. Sargent, P. harrosin, A. Sturk, T.G. van Leeuwen, R. Nieuwland, Particle size distribution of exosomes and microvesicles determined by transmission electron microscopy, flow cytometry, nanoparticle tracking analysis, and resistive pulse sensing, J. Thromb. Haemost. 12 (2014) 1182-1192 DOI: 10.1111/jth.12602

[20] V. Pospichalova, J. Svoboda, Z. Dave, A. Kotrbova, K. Kaiser, D. Klemova, L. Ilkovics, A. Hampl, I. Crha, E. Jandakova, L. Minar, V. Weinberger, V. Bryja, Simplified protocol for flow cytometry analysis of fluorescently labeled exosomes and microvesicles using dedicated flow cytometer, J. Extracell. Vesicles 4 (2015) 25530 http://dx.doi.org/10.3402/jev.v4.25530

[21] J. Caradec, G. Kharmate, E. Hosseini-Beheshti, H. Adomat, M. Gleave, E. Guns, Reproducibility and efficiency of serum-derived exosome extraction methods, Clin. Biochem. 47 (2014) 1286-1292 doi: 10.1016/j.clinbiochem.2014.06.011

[22] X. Osteikoetxea, A. Balogh, K. Szabó-Taylor, A. Németh, T.G. Szabó, K. Pálóczi, B. Sódar, Á. Kittel, B. György, É. Pállinger, J. Márkó, E.I. Buzás, Improved characterization of EV preparations based on protein to lipid ratio and lipid properties, PLoS ONE (2015) 10(3):e0121184. doi:10.1371/journal.pone.0121184

[23] I. Tatischeff, E. Larquet, J.M. Falcon-Pérez, P-Y. Turpin, S.G. Kruglik, Fast characterisation of cell-derived extracellular vesicles by nanoparticles tracking analysis, cryo-electron microscopy, and Raman tweezers microspectroscopy, Journal of Extracellular Vesicles 1 (2012) 19179. http://dx.doi.org/10.3402/jev.v1i0.19179

[24] Z.J. Smith, C. Lee, T. Rojalin, R.P. Carney, S. Hazari, A. Knudson, K. Lam, H. Saari, E. Lazaro Ibanez, T. Viitala, T. Laaksonen, M. Yliperttula, S. Wachsmann-Hogiu, Single

exosome study reveals subpopulations distributed among cell lines with variability related to membrane content, Journal of Extracellular Vesicles 4 (2015) 28533. http://dx.doi.org/10.3402/jev.v4.28533

[25] S. Stremersch, M. Marro, B-E. Pinchasik, P. Baatsen, A. Hendrix, S.C. De Smedt, P. Loza-Alvarez, A.G. Skirtach, K. Raemdonck, K. Braeckmans, Identification of Individual Exosome-Like Vesicles by Surface Enhanced Raman Spectroscopy. Small, doi: 10.1002/smll.201600393

[26] http://www.merckmillipore.com/HU/hu/life-science-research/protein-detection-quantification/direct-detect-spectrometer download at 2016.01.07.

[27] Mantsch, H. H. 2006. Biomedical Spectroscopy: Introduction. Encyclopedia of Analytical Chemistry, Published Online: 15 SEP 2006 DOI: 10.1002/9780470027318.a0101

[28] K-Z. Liu, R.A. Shaw, A. Man, T.C. Dembinski, H.H. Mantsch, Reagent-free, simultaneous determination of serum cholesterol in HDL and LDL by infrared spectroscopy, Clin. Chem. 48 (2002) 499-506.

[29] A. Dogan, P. Lasch, C. Neuschl, M.K. Millrose, R. Alberts, K. Schughart, D. Naumann, G.A. Brockmann, ATR-FTIR spectroscopy reveals genomic loci regulating the tissue response in high fat diet fed BXD recombinant inbred mouse strains. BMC Genomics 14 (2013) 386-403.

[30] S. Navarro, D. Borchman, E. Bicknell-Brown, Lipid-protein ratios by infrared spectroscopy, Anal Biochem 136 (1984) 382-389.

[31] C.J.B. daCosta, J.E. Baezinger, A rapid method for assessing lipid:protein and detergent:protein ratios in membrane-protein crystallization, Acta Cryst. D59 (2003) 77-83.

[32] B. Szalontai, Y. Nishiyama, Z. Gombos, N. Murata, Membrane dynamics as seen by Fourier transform infrared spectroscopy in a cyanobacterium, Synechocystis PCC 6803. The effect of lipid insaturation and the protein-to-lipid ratio, Biochim. Biophys. Acta 1509 (2000) 409-419.

[33] C. Ariöz, H. Götzke, L. Lindholm, J. Eriksson, K. Edwards, D.O. Daley, A. Barth, A. Wieslander, Heterologous overexpression of a monotopic glucosyltransferase (MGS) induces fatty acid remodeling in Escherichia coli membranes, Biochim. Biophys. Acta 1838 (2014) 1862–1870.

[34] T.J. Greenwalt, The how and why of exocytic vesicles, Transfusion 46 (2006) 143–152. doi:10.1111/j.1537-2995.2006.00692.x

[35] M. Franquesa, M.J. Hoogduijn, E. Ripoll, F. Luk, M. Salih, M.G.H. Betjes, J. Torras, C.C. Baan, J.M. Grinyó, A.M. Merino, Update on controls for isolation and quantification methodology of extracellular vesicles derived from adipose tissue mesenchymal stem cells, Front. Immunol. 5 (2014) 525 http://journal.frontiersin.org/article/10.3389/fimmu.2014.00525

[36] E. Goormaghtigh, V. Cabiaux, J.M. Ruysschaert, Determination of soluble and membrane protein structure by Fourier transform infrared spectroscopy. III. Secondary structures, Subcell. Biochem. 23 (1994) 405–450.

[37] A. Barth, Infrared spectroscopy of proteins, Biochim. Biophys. Acta 1767 (2007) 1073–1101.

[38] P. Schwinte, V. Ball, B. Szalontai, Y. Haikel, J.-C. Voegel, P. Schaaf, Secondary structure of proteins adsorbed onto or embedded in polyelectrolyte multilayers, Biomacromolecules 3 (2002) 1135-1143.

[39] E. Goormaghtigh, J. De-Meuter, B. Van Ioo, R. Brasseur, M. Rosseneu,J.M. Ruysschaert, Evaluation of the secondary structure of apo B-100 in low-density lipoprotein (LDL) by infrared spectroscopy, Biochim. Biophys. Acta 1006 (1989) 147-150.

[40] K. Smith, P.I. Haris, D. Chapman, K.B.M. Reid, S.J. Perkins, β-Sheet secondary structure of the trimeric globular domain of C1q of complemet and collagen types VIII and X by Fourier-transform infrared spectroscopy and averaged structure predictions, Biochem. J. 301 (1994) 249-256.

[41] E.B. Brauns, R.B. Dyer, Time-Resolved Infrared Spectroscopy of RNA folding, Biophys. J. 89 (2005) 3523-3530 doi:10.1529/biophysj.105.061531

[42] J.A. Knight, S. Anderson, J.M. Rawle, Chemical basis of the sulfo-phospho-vanillin reaction for estimating total serum lipids, Clinical Chem. 18 (1972) 199-202.

[43] M. Goldberg, A.F. Chafotte, Undistorted structural analysis of soluble proteins by attenuated total reflectance infrared spectroscopy, Protein Sci. 2005 Nov; 14(11): 2781–2792 doi: 10.1110/ps.051678205

[44] T.L. Steck, The organization of proteins in the human red blood cell membrane, J. Cell. Biol. 62 (1974) 1-19.

[45] R. Deák, J. Mihály, I.Cs. Szigyártó, A. Wacha, G. Lelkes, A. Bóta, Physicochemical characterization of artificial nanoerythrosomes derived from erythrocyte ghost membranes, Coll. Surf. B 135 (2015) 225-234.

Supplementary material

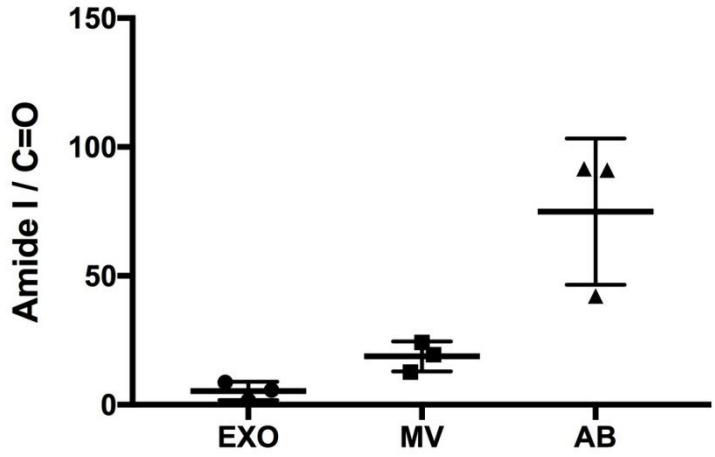

Fig.S1. Relative intensities of amide I and lipid-related carbonyl stretching bands for Jurkat cell line derived EVs. Mean values are presented by horizontal lines, error bars mark denotes the standard error of the mean (SEM).

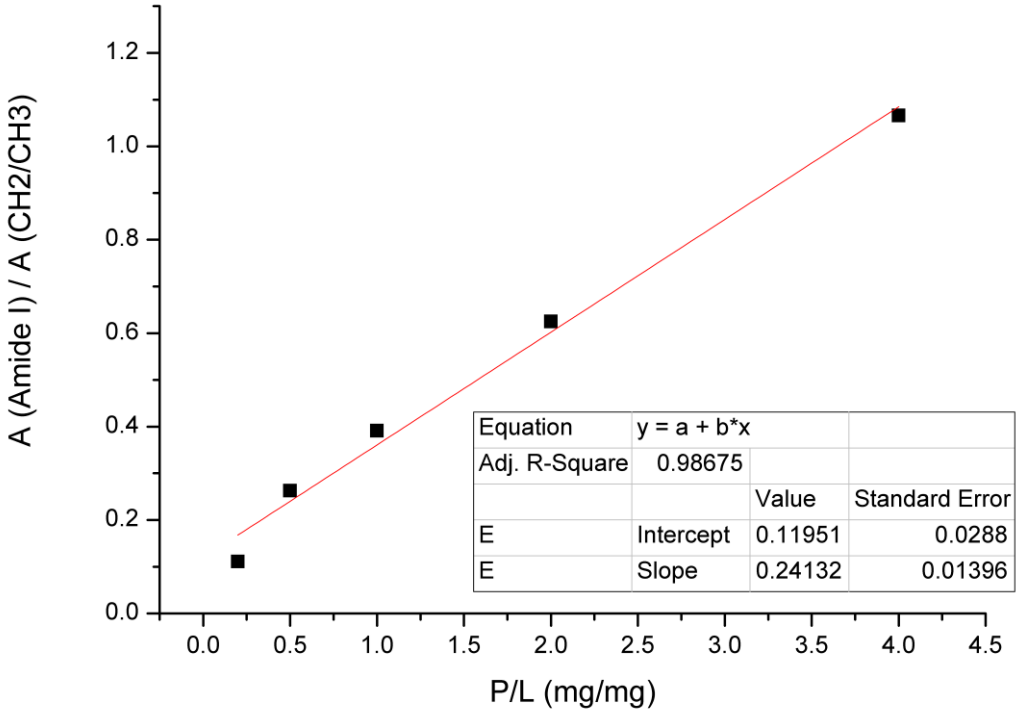

Fig.S2. Ratios of integrated area of selected amide I band and of C-H stretching region (**A (Amide I) / A (CH2/CH3)**) for BSA-lipid (Chol:DPPC:DOPC:DPPE:DPPS=5:1:1:2:1) mixtures of varying relative content.

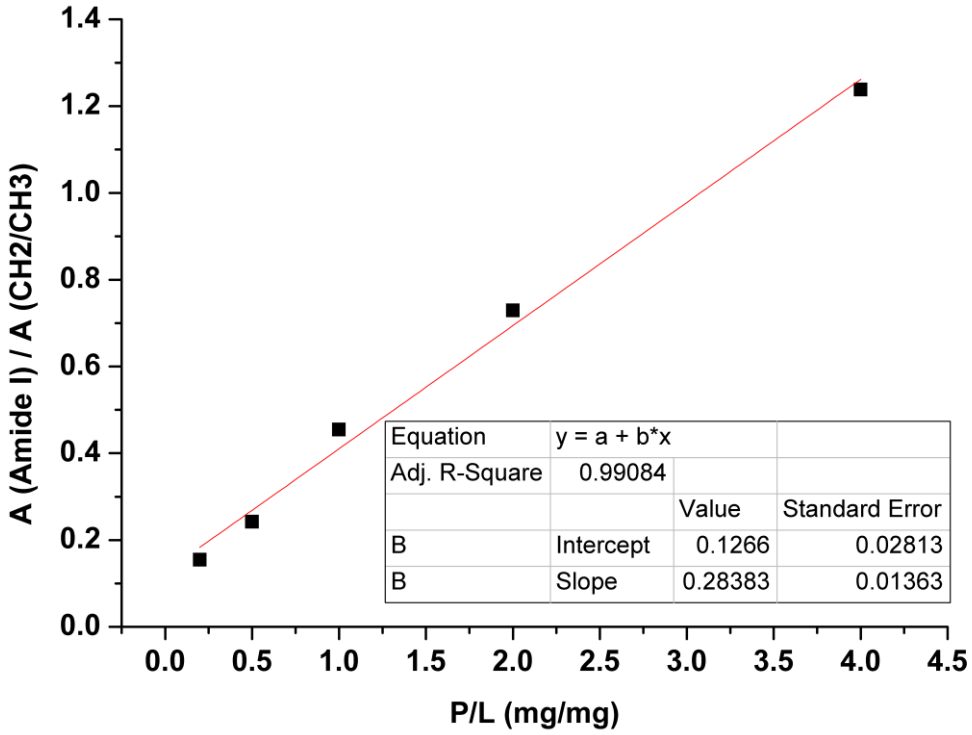

Fig. S3. Ratios of integrated area of selected amide I band and of C-H stretching region (**A (Amide I) / A (CH2/CH3)**) for BSA-Brain Total Lipid Extract mixtures of varying relative content.

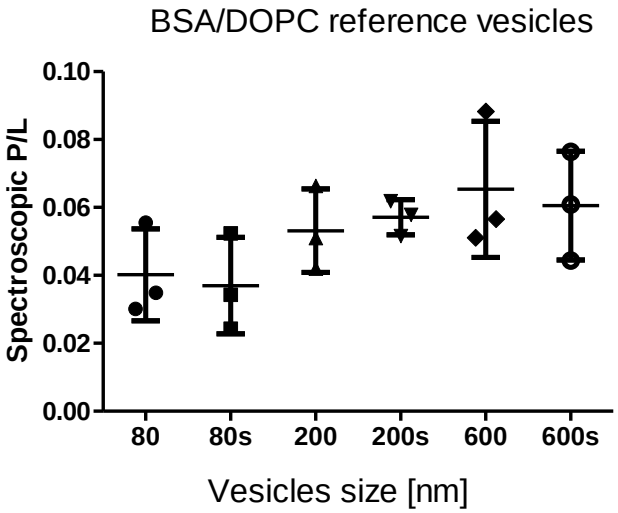

Fig.S4. Calculated P/L_{spectr} values for BSA/DOPC reference vesicles with different mean diameter size (600, 200 and 80 nm) before and after sonication treatment (s indices sonication). Mean values are presented by horizontal lines, error bars mark the standard error of the mean (SEM).

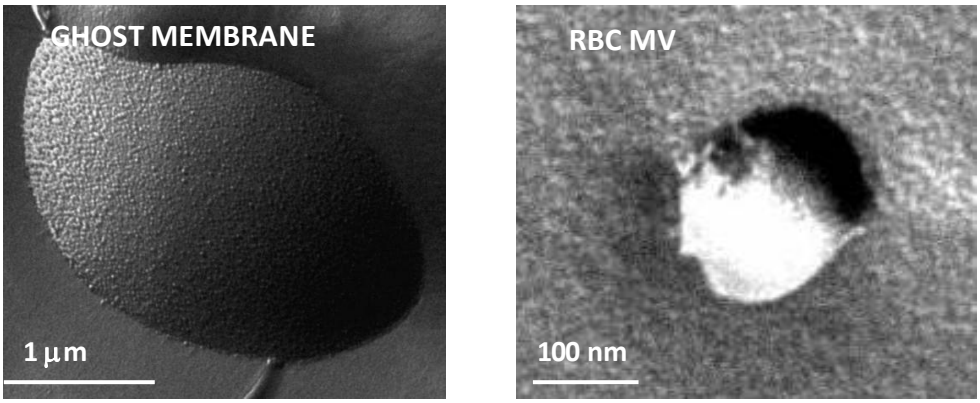

Fig.S5. FF-TEM picture of RBS ghost membrane and that of RBC derived MV.

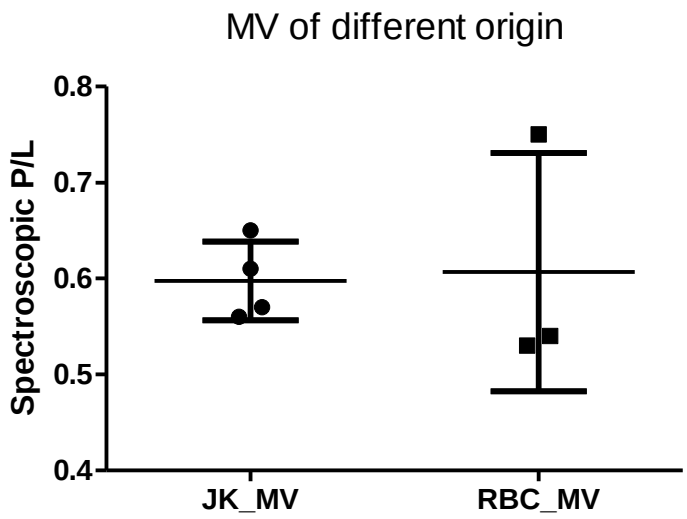

Fig.S6. Calculated P/L_{spectr} values of MV subpopulations of different origin: JK_MV - Jurkat cell derived microvesicles, RBC_MV - red blood cell derived microvesicles. Mean values are presented by horizontal lines, error bars mark the standard error of the mean (SEM).

Table S1. Results of one-way ANOVA of unpaired t-test data obtained on values of relative intensities of amide I and lipid-related carbonyl stretching bands for Jurkat cell line derived EXO, MV and AB vesicles

Number of families	**1**					
Number of comparisons per family	**3**					
Alpha	**0,05**					
Tukey's multiple comparisons test	**Mean Diff.**	**95.00% CI of diff.**	**Significant?**	**Summary**	**Adjusted P Value**	
EXO vs. MV	**-13,42**	**-55.64 to 28.79**	**No**	**ns**	**0,6172**	**A-B**
EXO vs. AB	**-69,58**	**-111.8 to -27.36**	**Yes**	******	**0,0056**	**A-C**
MV vs. AB	**-56,16**	**-98.37 to -13.94**	**Yes**	*****	**0,0153**	**B-C**
Test details	**Mean 1**	**Mean 2**	**Mean Diff.**	**SE of diff.**	**n1**	**n2**
EXO vs. MV	**5,34**	**18,76**	**-13,42**	**13,76**	**3**	**3**
EXO vs. AB	**5,34**	**74,92**	**-69,58**	**13,76**	**3**	**3**
MV vs. AB	**18,76**	**74,92**	**-56,16**	**13,76**	**3**	**3**

Table S2. Results of one-way ANOVA of unpaired t-test data obtained on relative intensities of amide I and lipid-related carbonyl stretching bands for Jurkat cell line derived EXO, MV and AB vesicles

Table Analyzed	Unpaired t test data					
One-way analysis of variance						
P value	< 0,0001					
P value summary	****					
Are means signif. different? (P < 0.05)	Yes					
Number of groups	3					
F	64,35					
R square	0,9346					
ANOVA Table	SS	df	MS			
Treatment (between columns)	0,7615	2	0,3807			
Residual (within columns)	0,05325	9	0,005917			
Total	0,8147	11				
Bonferroni's Multiple Comparison Test	Mean Diff	t	Significan	Summary	95% CI of diff	
JK-EXO vs JK-MV	0,1975	3,631	Yes	*	0,03796 to 0,3570	
JK-EXO vs JK-AB	-0,4075	7,492	Yes	***	-0,5670 to -0,2480	
JK-MV vs JK-AB	-0,605	11,12	Yes	****	-0,7645 to -0,4455	

Table S3. Results of unpaired t-test data obtained on P/L spectr values for MV vesicles of different origin (Jurkat cell and red blood cell). derived from relative intensities of amide I and C-H stretching bands

Table Analyzed	Unpaired t test data
Column A	JK_MV
vs	vs
Column B	RBC_MV
Unpaired t test	
P value	0,893
P value summary	ns
Are means signif. different? (P < 0.0	No
One- or two-tailed P value?	Two-tailed
t, df	t=0,1416 df=5
How big is the difference?	
Mean ± SEM of column A	0,5975 ± 0,02056 N=4
Mean ± SEM of column B	0,6067 ± 0,07172 N=3
Difference between means	-0,009167 ± 0,06475
95% confidence interval	-0,1757 to 0,1573
R square	0,003992
F test to compare variances	
F,DFn, Dfd	9,123, 2, 3
P value	0,1061
P value summary	ns
Are variances significantly different	No

Table S4. Results of one-way ANOVA of unpaired t-test data obtained on P/L_{spectr} values for BSA/DOPC reference vesicles with different mean diameter size (600, 200 and 80 nm).

Table Analyzed	Unpaired t test data					
One-way analysis of variance						
P value	0,1689					
P value summary	ns					
Are means signif. different? (P < 0.05)	No					
Number of groups	6					
F	1,895					
R square	0,4413					
ANOVA Table	SS	df	MS			
Treatment (between columns)	0,001931	5	0,0003862			
Residual (within columns)	0,002445	12	0,0002037			
Total	0,004376	17				
Bonferroni's Multiple Comparison Test	Mean Diff,	t	Significant? P < 0,05	Summary	95% CI of diff	
80 vs 80mw	0,003199	0,2745	No	ns	-0,03933 to 0,04572	
80 vs 200	-0,01298	1,114	No	ns	-0,05551 to 0,02955	
80 vs 200mw	-0,01694	1,454	No	ns	-0,05947 to 0,02558	
80 vs 600	-0,02516	2,159	No	ns	-0,06769 to 0,01737	
80 vs 600mw	-0,02037	1,748	No	ns	-0,06290 to 0,02215	
80mw vs 200	-0,01618	1,388	No	ns	-0,05871 to 0,02635	
80mw vs 200mw	-0,02014	1,728	No	ns	-0,06267 to 0,02238	
80mw vs 600	-0,02836	2,433	No	ns	-0,07088 to 0,01417	
80mw vs 600mw	-0,02357	2,022	No	ns	-0,06610 to 0,01896	
200 vs 200mw	-0,003964	0,3401	No	ns	-0,04649 to 0,03856	
200 vs 600	-0,01218	1,045	No	ns	-0,05470 to 0,03035	
200 vs 600mw	-0,00739	0,6341	No	ns	-0,04992 to 0,03514	
200mw vs 600	-0,008214	0,7048	No	ns	-0,05074 to 0,03431	
200mw vs 600mw	-0,003427	0,294	No	ns	-0,04595 to 0,03910	
600 vs 600mw	0,004788	0,4108	No	ns	-0,03774 to 0,04731	

Figure and table captions:

Table 1. Total protein content (with standard deviations) of Jurkat cell derived EV subpopulations (n=4 independent isolation).

Table 2. Spectroscopic protein-to-lipid values calculated for Jurkat cell line derived EVs. JK(1-4) refer to the 4 independent EV isolations. A(Amide I) and A(CH2/CH3) denote the integrated area of selected amide I band and that of C-H stretching region characteristic for protein and lipid components, respectively.

Table 3. Spectroscopic protein-to-lipid values calculated for red blood cell (RBC) derived MVs (3 independent isolations: RBC1-RBC3), compared with that of ghost membrane prepared from the same RBS concentrate.

Table S1. Results of one-way ANOVA of unpaired t-test data obtained on values of relative intensities of amide I and lipid-related carbonyl stretching bands for Jurkat cell line derived EXO, MV and AB vesicles

Table S2. Results of one-way ANOVA of unpaired t-test data obtained on IR based protein-to-lipid ratio values for Jurkat cell derived EXO, MV and AB vesicles

Table S3. Result unpaired t-test data obtained on IR based protein-to-lipid ratio values for MV vesicles of different origin (Jurkat cell and red blood cell).

Table S4. **Re**sults of one-way ANOVA of unpaired t-test data obtained on P/L_{spectr} values for BSA/DOPC reference vesicles with different mean diameter size (600, 200 and 80 nm).

Fig.1 (A) Typical FF-TEM pictures of Jurkat cell derived EV subpopulations. (B) Size distribution measured by dynamic light scattering (DLS) measured for the same EV subpopulations. D: mean diameter; P.d.: polydispersity.

Fig.2 (A) Representative ATR-FTIR spectra of EVs isolated by differential centrifugation from Jurkat cell line. (B) Representative ATR-FTIR spectra of EVs after PBS buffer subtraction in the 1800-1350 cm^{-1} wavenumber region: C=O stretching from lipid esters, amide I and amide II bands of proteins. (C) Second derivative IR spectra of the amide I region for protein secondary structure assessing.

Fig.3 Selected wavenumber regions of a 'contaminated' Jurkat cell derived exosome (isolation JK4) used for P/L determination protocol: (A) Amide I and amide II wavenumber region (1770-1470 cm^{-1}) deconvoluted by curve fitting with Lorentz-function (band denoted by dotted lines), (B) C-H stretching region (3040-2700 cm^{-1}) acting for lipid components.

Fig.4 Protein-to-lipid ratio calculated from IR spectra of Jurkat cell line derived EVs. Mean values are presented by horizontal lines, error bars mark denotes the standard error of the mean (SEM).

Fig.5 (A) Representative ATR-FTIR spectrum of RBC derived MV (blue line) compared with RBC ghost membrane spectrum (red line). (B) Second derivative IR spectra of the amide I region for protein secondary structure assessing.

Fig.S1. Relative intensities of amide I and lipid-related carbonyl stretching bands for Jurkat cell line derived EVs. Mean values are presented by horizontal lines, error bars mark denotes the standard error of the mean (SEM).

Fig.S2. Ratios of integrated area of selected amide I band and of C-H stretching region (**A (Amide I) / A (CH2/CH3)**) for BSA-lipid (Chol:DPPC:DOPC:DPPE:DPPS=5:1:1:2:1) mixtures of varying relative content.

Fig. S3. Ratios of integrated area of selected amide I band and of C-H stretching region (**A (Amide I) / A (CH2/CH3)**) for BSA-Brain Total Lipid Extract mixtures of varying relative content.

Fig.S4. Calculated P/L_{spectr} values for BSA/DOPC reference vesicles with different mean diameter size (600, 200 and 80 nm) before and after sonication treatment (s indices sonication). Mean values are presented by horizontal lines, error bars mark the standard error of the mean (SEM).

Fig.S5. FF-TEM picture of RBS ghost membrane and that of RBC derived MV.

Fig.S6. Calculated P/L_{spectr} values of MV subpopulations of different origin: JK_MV - Jurkat cell derived microvesicles, RBC_MV - red blood cell derived microvesicles.